Document downloaded from:

http://hdl.handle.net/10251/157196

This paper must be cited as:

Ullah, S.; Bouich, A.; Ullah, H.; Vega-Fleitas, E.; Baig, F.; Hameed, Y.; Mollar García, MA.... (2019). Influence of Fe Content in Binary SnS2 Synthesis by Hydrothermal Technique for Photovoltaic Application. Journal of The Electrochemical Society. 8(6):Q118-Q122. https://doi.org/10.1149/2.0251906jss

The final publication is available at

https://doi.org/10.1149/2.0251906jss

Copyright The Electrochemical Society

Additional Information

ECS Journal of Solid State Science and Technology, **8** (6) Q118-Q122
[DOI: 10.1149/2.0251906jss]

Influence of Fe content in binary SnS_2 synthesis by hydrothermal technique for photovoltaic application.

Shafi Ullah [a,b], Amal Bouich [a], Hanif Ullah [b], Erika Vega Fleitas[a], Faisal Baig [a,b], Yousaf Hameed [a,b], Miguel Mollar [a], Bernabé Marí [a].

[a] *Department of Applied Physics-IDF, Universitat Politècnica de València, València, Spain*

[b] *Department of Electrical Engineering, Federal Urdu University of Arts, Science and Technology, Islamabad, Pakistan*

Corresponding author: shafi399@yahoo.com

Abstract.

Binary thin disulfide (SnS_2) and ternary $Sn_{1-x}Fe_xS_2$ (X = Fe (2.5%, 5% and 10%) which has huge potentials in the visible-light rang due to its band gap 2.2-2.6 eV. Herein, SnS_2 and $Sn_{1-x}Fe_xS_2$ powders have been synthesize by a fruitful hydrothermal method. The structure, morphology, elemental composition and optical properties of the obtained product were characterized by using X-ray diffraction (XRD), Field Emission Scanning Electron Microscopy (FESEM), Electron Dispersive Spectroscopy (EDS) and UV-Vis spectroscopy. It was found that the Fe could be effectively incorporated in the obtained $Sn_{1-x}Fe_xS_2$ compounds. According to XRD analysis, increased concentration of Fe in the $Sn_{1-x}Fe_xS_2$ compounds results in a gradual degradation of the crystallinity. The optical bandgap was found to be 1.52 eV, 2.22 eV, 2.38 eV and 2.48 eV, for the SnS, SnS_2, Fe 5% and Fe 10% respectively. Mott–Schottky measurements performed for SnS_2 confirm the n-type character of SnS_2 samples.

Key words: SnS_2, Fe doped, XRD, FESEM, EDS, Optical and Mott-Schottky analysis.

ECS Journal of Solid State Science and Technology, **8** (6) Q118-Q122
[DOI: 10.1149/2.0251906jss]

Introduction

Recently, fabrication of environmental friendly, low cost-effective and highly efficient solar cells has been an increasing interest in the research area. This includes the preparation of both absorber and buffer layers using high abundance and low environmental hazardous elements [1]. A significant improvement was achieved by substituting Cu (In, Ga) Se_2, CdTe) with earth-abundant absorber layers such as Cu_2ZnSnS_4 (CZTS), Cu_2SnS_3 (CTS) and SnS. But little attention has been paid among the sulfide binary semiconductor buffer layer, till to date, CdS which has a band gap of about 2.42 eV is the best efficiencies are achieved with CdS buffer layer [2]. However, on the other side alternative binary buffer materials such as In_xSe_y [3], ZnS [4], In_2S_3 [5], Al_2O_3 [6], ZnSe [7] and ZnO [8] are reported.

The efficiency of the CdS buffer layer device still lags. As day by day increasing considerable interest as promising buffers layer Sn based compound SnO_2, Sn (O, S) and SnS_2 [9] have been attracted to replace with conventional toxic CdS. In addition, tin based buffer layers expected to help for the formation of the junction between the window and absorber layer [10]. Furthermore, using the wide band gap Sn based buffer layers, to maximize the amount of incident light to the junction region in order to make full use of solar spectrum. Moreover, it has a suitable band gap 2.2 eV to transmit most of the solar radiation to the absorber layer [11].

SnS_2 can be used for various application like, electrical switches, quantum well structure and recording system [12], different rang of physical and chemical methods have been reported to prepare SnS_2 such as, chemical vapour deposition [13], spray pyrolysis [14], Chemical bath deposition (CBD) [15], plasma-enhanced chemical vapour deposition (PECVD) [16] and dip deposition [17].

In this work we report, hydrothermal low-cost method for synthesis of SnS_2 product using common, nontoxic $SnCl_45H_2O$ and thioacetamide as the reactants and 5 % acetic acid aqueous solution as the solvent and the influence of Fe content at different (2.5%, 5%, 10%). The structure, composition and optical property of the resultant products were characterized by X-ray diffraction (XRD), Field emission surface electron microscopy (FESEM), energy dispersive spectroscopy (EDS) and UV–Vis transmittance measurement spectra.

Experimental

All chemicals and reagents were used directly without further purification as received. Absolute ethanol, isopropyl alcohol, acetone, Analytical grade stannic chloride pentahydrate ($SnCl_4.5H_2O$) and thioacetamide (C_2H_5NS) were bought from Sigma-Aldrich.

SnS_2 and $Sn_{1-x}Fe_xS_2$ (with x = 2.5%, 5% and 10%) were prepared using the required amounts of analytical grade tin (IV), iron ($FeCl_3$) and thioacetamide were weighted as described by Elsevier [18]. The SnS_2 powders were synthesized by hydrothermal method according to a slightly modified method reported by Li et al [19]. After the reaction system cooled down at room temperature. finally, the yellow products were collected by centrifugation and well washed by alcohol and distilled water for 3 times before drying in a vacuum dried at 100 ºC for 3 hours.

The crystal structure of SnS_2 and different Fe at (2.5%, 5%, 10%) composite were investigated by X-ray diffraction (XRD) using a Rigaku Ultima IV diffractometer in the Bragg-Brentano configuration using CuKα radiation (λ = 1.54060 Å). Chemical composition, surface morphology and topography were characterized using energy dispersive spectroscopy (EDS) and field emission scanning electron microscopy (FESEM) a Zeiss ULTRA 55 model equipped with an In-Lens SE detector respectively.

Optical properties of SnS and SnS_2 films were measured at room temperature by using IR-VIS-UV spectrophotometer at wavelength within the range (400–900) nm. Mott–Schottky measurements were performed using Autolab potentiostat PGSTAT302N [20].

1. Results and discussion

Figure 1 shows the XRD patterns of SnS_2 and $Sn_{1-x}Fe_xS_2$ with various amount of Fe (x=2.5, 5 and 10%). Several diffraction peaks located at 14.95º, 28.29º, 30.20º, 32.12º, 46.00º, 50.00º, 52.47º, 58.55º and 59.62º respectively, corresponding to the lattice planes (001), (100), (002), (101), (003), (110), (111), (200) and (112) are displayed in the XRD diffractogram. These diffraction peaks match very well with the reference standard card (JCPDS NO- 23–677) corresponding to Berndtite structure of SnS_2.

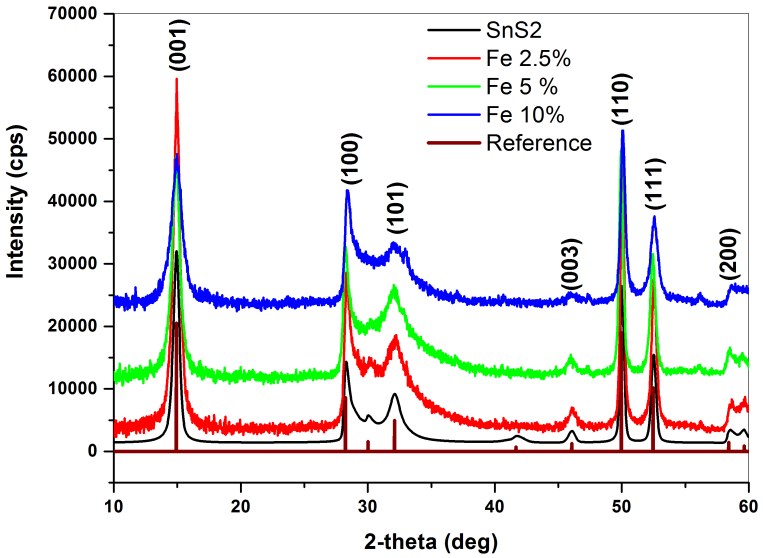

Figure 1. X-ray diffraction patterns of SnS_2 and $Sn_{1-X}Fe_xS_2$ (x = 2.5%, 5%,10%).

XRD peaks for the binary SnS_2 and ternary $Sn_{1-X}Fe_xS_2$ (with Fe contents 2.5%, 5% and 10%) are found to be located at the same 2θ angles meaning that the crystalline structure is maintained, and the Fe atoms locate at Sn sites. Two main effects are observed with the increase of Fe contents. First, the intensity of diffraction peaks drops, which means that the crystallinity of the ternary $SnFeS_2$ compounds decreases with the Fe content. Second, the XRD peaks become broader when increasing Fe concentration. This effect is related to a smaller in size of the crystallites. This result is further verified by measuring the Full Width at Half Maximum (FWHM) of XRD peaks. From the FWHM the crystallite size is calculated according to the Scherrer equation [21],

$$D = \frac{K\lambda}{\beta Cos\theta}$$

where β is the full width at half maximum (FWHM), λ is the X-ray wavelength having a value of 1.5418 Å (CuKα), K is a proportionality constant (K = 0.9 was used) and θ is the Bragg angle at the Centre of the peak. The crystallite size D is the size of the crystal in the perpendicular direction to the reflecting planes.

The crystallite size calculated for the XRD peak (001) peak is shown in Table 1. As expected, the higher the Fe contents the smaller the crystallite size. Figure 2 shows the

variation of FWHM and crystallite size relation along the (001) peak with different Fe contents. Furthermore, as increases the dopant concentration from 0% to 10% the position of the diffraction peaks slightly shifts to higher angles. Sn^{2+} ions (140 pm) are been substituted by smaller radius in size Fe^{2+} ions (126 pm) and then diffraction planes are closer and diffraction peaks shifts to higher angles [22].

Simples ID	***2θ for (001) peak (degree)***	***FWHM (degree)***	***Crytallite size (nm)***
SnS_2	14.93	0.56	58.2
SnS_2 ; Fe 2.5%	14.93	0.65	49.9
SnS_2 ; Fe 5%	14.93	0.71	46.2
SnS_2 ; Fe 10%	14.93	0.73	44.5

Table 1. represent the SnS_2 crystallite size with different Fe contents.

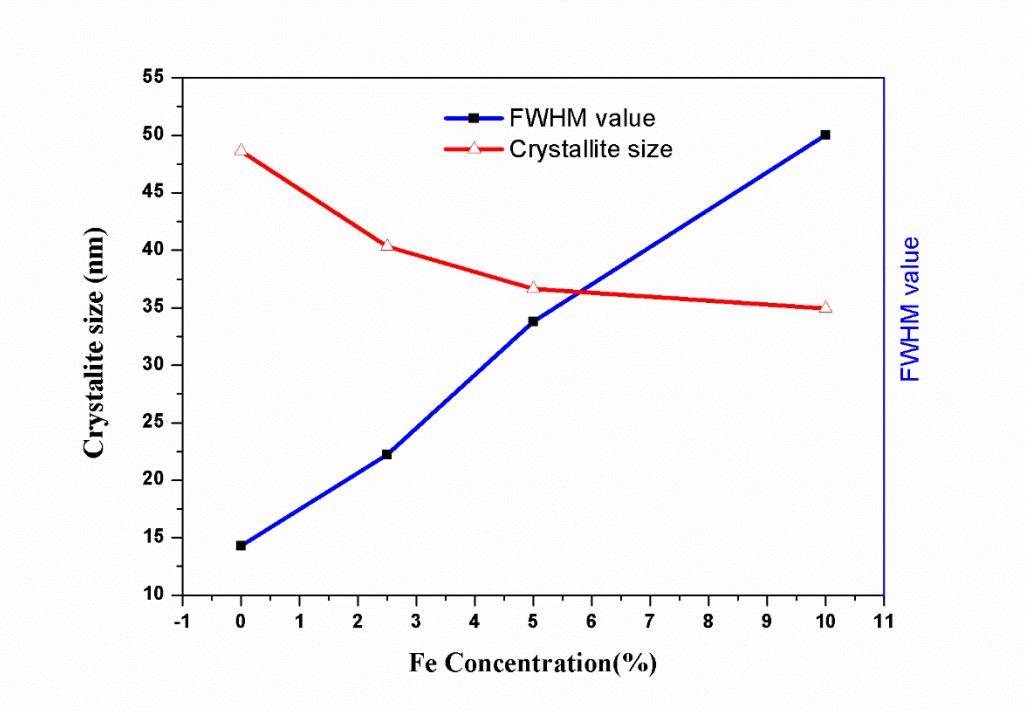

Figure 2. Variation of crystallite size with FWHM value with different Fe (0, 2.5, 5 and 10%) contents.

Figure 3 shows the surface morphology of the as-synthesized SnS_2 and $SnFeS_2$ powders as observed from the FESEM images. The surface roughness decreases dramatically as increases the Fe contents, finer and more homogenous surface are formed. This provides again an evidence that different morphologies are indeed dependent on Fe/Sn ratio.

ECS Journal of Solid State Science and Technology, **8** (6) Q118-Q122
[DOI: 10.1149/2.0251906jss]

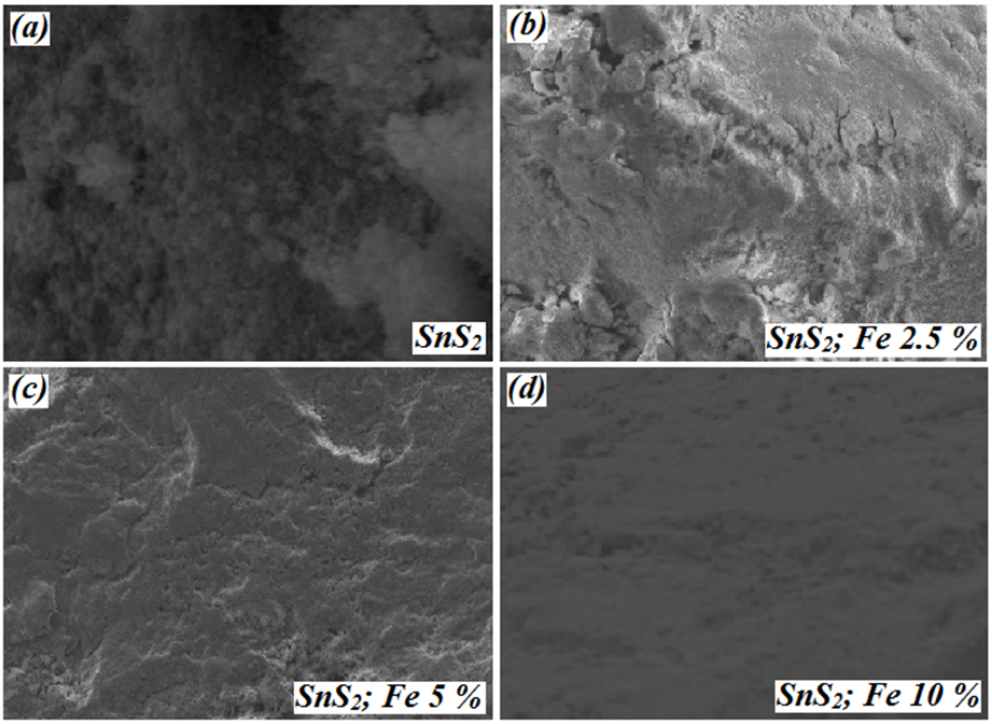

Figure 3. Top view FESEM images of SnS_2 prepared with different amount of additional Fe: (a) 0%, (b) 2.5%, (c) 5%, and (d) 10% content.

Figure 4 displays the elemental mapping of S, Sn, and Fe elements in $Sn_{1-X}Fe_xS_2$ powder. It can be observed that the elements are uniformly distributed in the $Sn_{1-X}Fe_xS_2$ compounds. This indicates that the elements are localized in the nanoparticle in random form and the ratio of Sn:S was calculated to be 1:2 [23], which further demonstrates that the obtained product is SnS_2 in Figure 4.

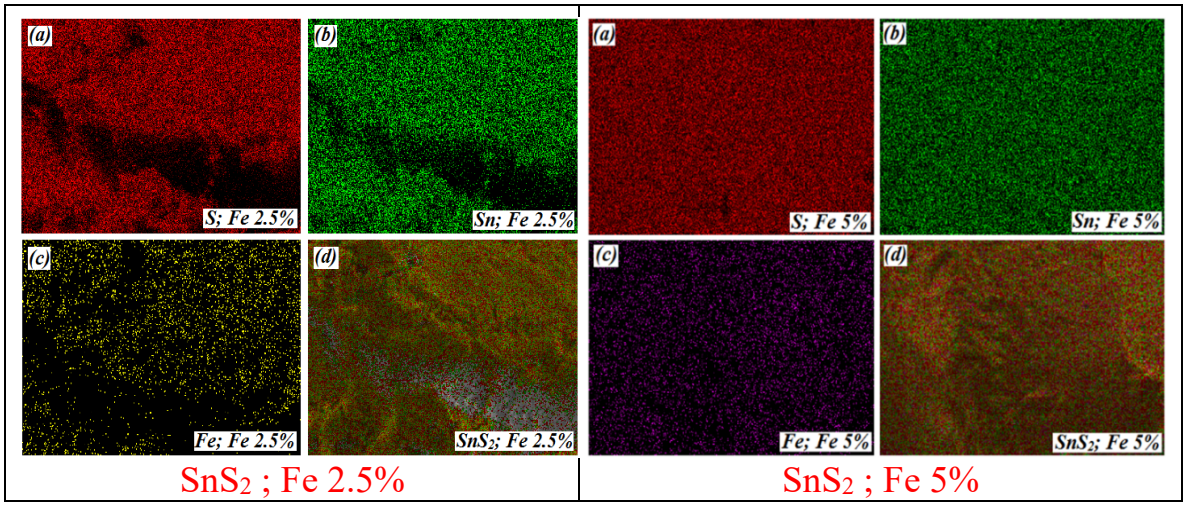

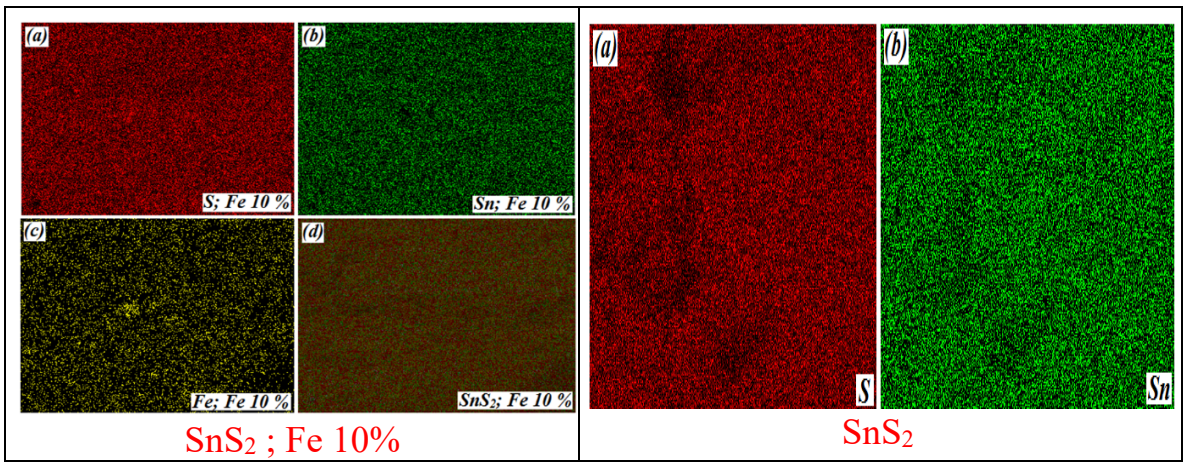

Figure 4. EDS mapping of $SnFeS_2$ compounds, elemental distribution of S, Sn, and Fe for various Fe contents (2.5%, 5%, 10%).

Typical EDS spectrum showing how characteristic X-rays correspond to different elements. It is clearly seen that the synthesized powders are mainly composed of S, Sn, and Fe elements, as shown in Table 2. As seen in the EDS spectra in Figure 5, no other peak related to impurity was detected from the elemental composition. This confirms that only Fe has been incorporated onto the SnS_2 surface.

Simples ID	***S %***	***Sn %***	***Fe %***	***Eg (eV)***
SnS_2	61.74	38.24	---------	2.22
SnS_2 ; Fe 2.5%	61.93	37.20	1.05	-------
SnS_2 ; Fe 5%	63.19	34.08	2.73	2.38
SnS_2 ; Fe 10%	61.22	32.60	6.18	2.48

Table 2. shows the EDS elemental composition of SnS_2 with addition of Fe content.

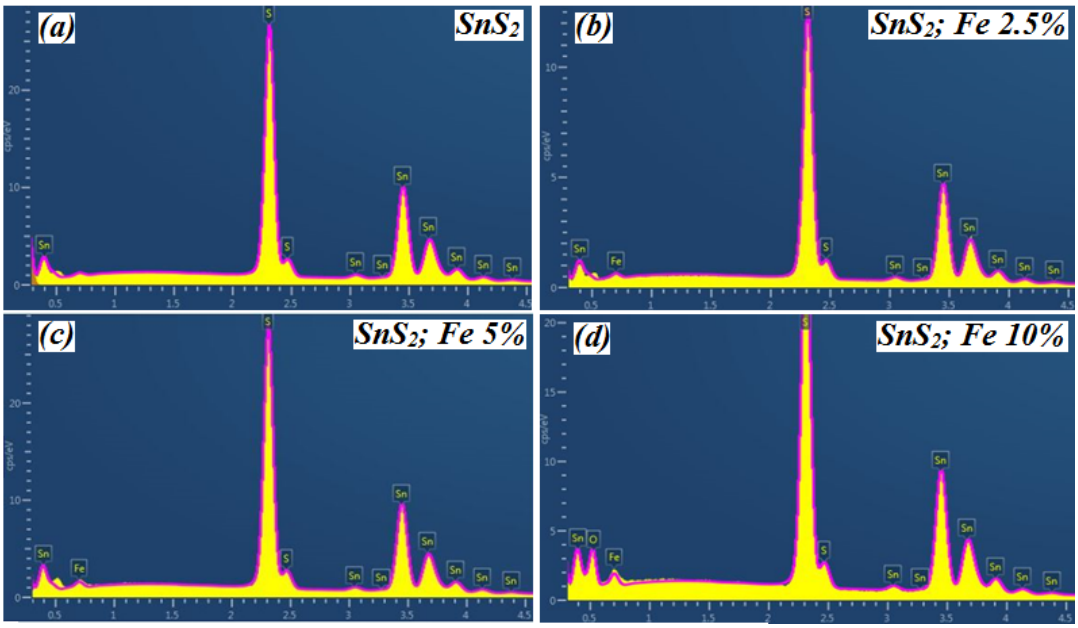

Figure 5. Elemental composition of $SnFeS_2$ with different Fe contents.

2. Optical analysis

The optical properties such as absorption coefficient, transmittance and band gap energy for SnS as a p-type material 1.52 eV to compare with SnS_2 n-type 2.22 eV material were determined. Figure 6 (a, b,) shows the optical transmittance and absorption versus the wavelength (λ) in the range 400–900 nm. An important shift to shorter wavelengths in the onset of the transmittance is observed for the SnS to SnS_2 composite. the SnS and SnS_2 semiconductors materials has a direct energy band gap [24]. Then the optical band gap of direct band gap semiconductors can be estimated from by plotting the square of absorbance times energy photon $(\alpha h\upsilon)^2$ versus the photon energy ($h\upsilon$). The point where the extrapolation of the straight-line portion to the energy axis at ($\alpha = 0$) is the value of the optical band gap. Figure 6 (c, d) shows Using the relation $\alpha^2 = A\ (E_g - h\upsilon)$, which is valid for this type of materials, Eg values of 1.52 eV, 2.22 eV, 2.38 eV and 2.48 eV were found, for the SnS, SnS_2, Fe 5% and Fe 10% respectively. The band gap shift is naturally related to decrease in carrier concentration as the increasing of iron contents. Furthermore, this variation in the optical absorption in the visible region corresponds to changes in both the crystalline quality and roughness of Fe-doping concentration.

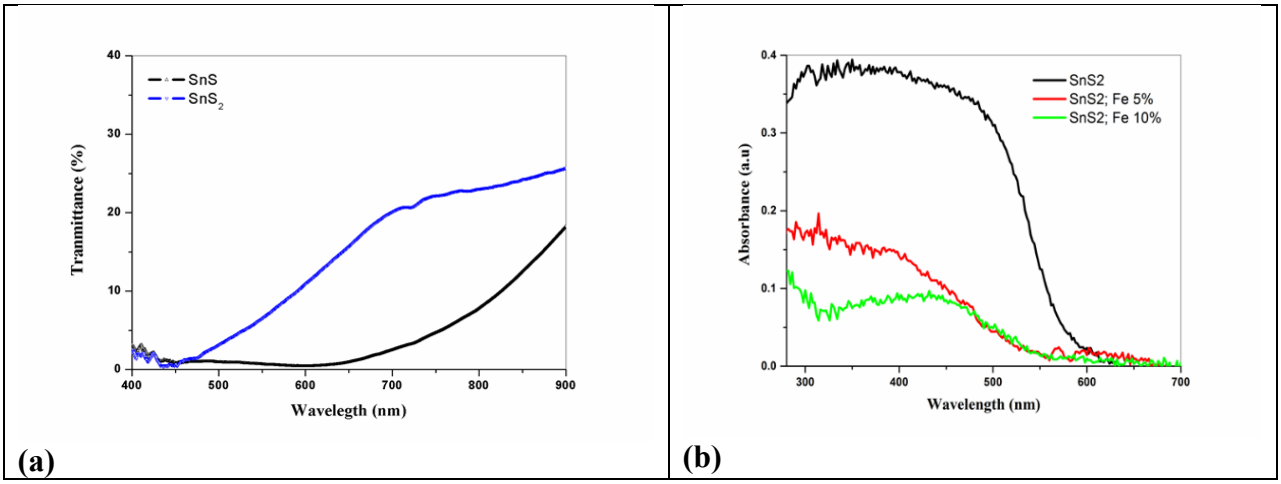

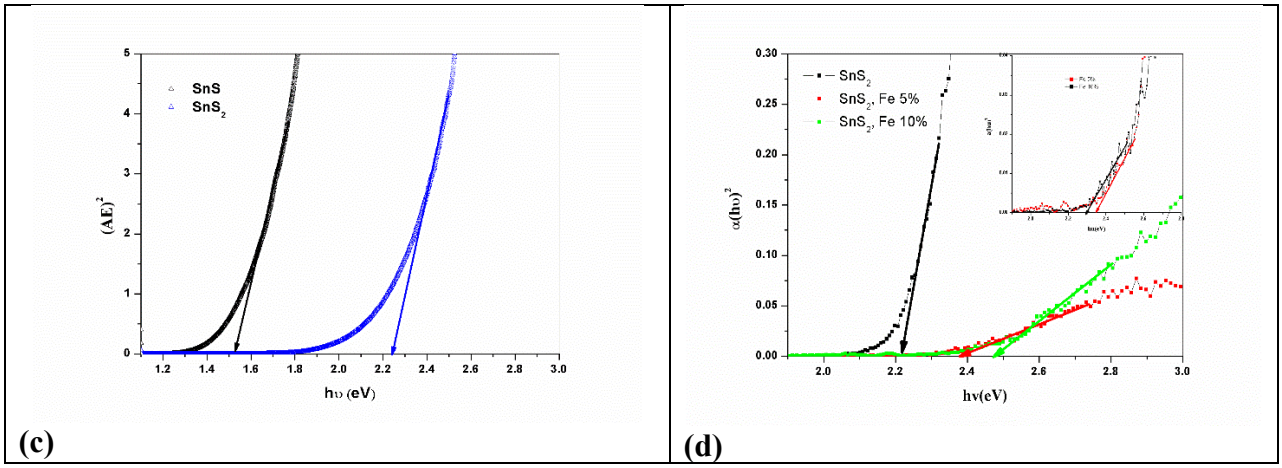

Figure 6. Optical transmittance of SnS and SnS_2(a), Absorbance of SnS_2 doped Fe % (b), Plot of $(AE)^2$ versus the photon energy (hν) for SnS and SnS_2 (c) and optical band gap of SnS_2 doped Fe content (d).

3. Mott–Schottky analysis

In figure 7 Mott–Schottky measurements were performed in a quartz cell using the Auto lab potentiostat PGSTAT302N with a Pt rod counter electrode, Ag/AgCl saturated in 3 M KCl reference electrode and working electrode is 0.25 cm^2 using 1 M of Na_2SO_4 electrolyte. The Mott–Schottky plot ($1/C^2$ vs applied potential) was obtained and analyzed for all the samples. The flat band potential is an important physical property as regard to the performance of the material in photoelectrochemical [25]. Both N_D and E_{fb} were estimated from the Mott-Schottky equations (Eqs. 1):

$$\frac{1}{{C_{SC}}^2} = \frac{2}{e\,\varepsilon\,\varepsilon_0 N_D {A_S}^2}\left(E - E_{fb} - \frac{KT}{e}\right) \text{ for n-type semiconductor} \quad \textbf{(1)}$$

where, e is the electron charge, ε is the dielectric constant of the semiconductor, εo is the vacuum permittivity, A_S is the surface area of the working electrode, k is the Boltzmann's constant, and T the temperature. The calculated value was found that the E_{fb} of the electrode using SnS_2 are about -0.68 V and -0.71 V (vs. SCE), respectively [26].

The positive slope confirm that SnS_2 is a n-type semi-conducting material which can be used as buffer layer for photovoltaic solar cells application. According to eq. 1 the estimated values for the concentration of donors were about: ND = 3.6×10^{18} (cm^{-3}).

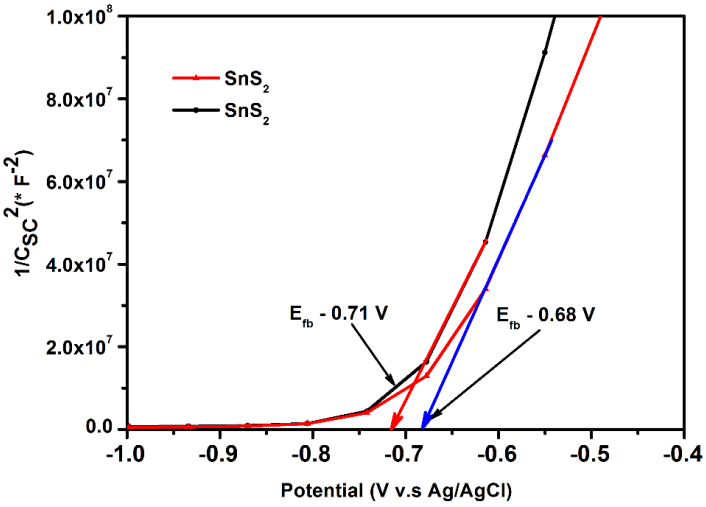

Figure 7. Mott-Schottky plots of an electrode using SnS_2 with 1 M Na_2SO_4 at a frequency of 1 KHz.

4. Conclusions

Binary SnS_2 and ternary $Sn_{1-X}Fe_xS_2$ (with x = 2.5%, 5% and 10%) compounds were prepared by simple hydrothermal technique of the precursor species, which is a novel procedure to prepare this type of compounds. The structure characterization was carried out through XRD measurements indicated the crystal size is Berndtite JCPDS card #: 23–677 without any secondary phases. The optical band gap values were obtained 1.52 eV, 2.22 eV, 2.38 eV and 2.48 eV for the SnS, SnS_2, Fe 5% and Fe 10% respectively. Mott–Schottky measurements was used to determine the type of conductivity, which was found to be n-type for SnS_2.

Acknowledgments

This work was supported by Ministerio de Economia y Competitividad (ENE2016-77798-C4-2-R).

References.

[1] Zhang, Yong Cai, Zhen Ni Du, Kun Wei Li, and Ming Zhang. "Size-controlled hydrothermal synthesis of SnS_2 nanoparticles with high performance in visible light-driven photocatalytic degradation of aqueous methyl orange." *Separation and Purification Technology* 81, no. 1 (2011): 101-107.

[2] Gedi, Sreedevi, Vasudeva Reddy Minnam Reddy, Babu Pejjai, Chinho Park, Chan-Wook Jeon, and Tulasi Ramakrishna Reddy Kotte. "Studies on chemical bath deposited SnS_2 films for Cd-free thin film solar cells." *Ceramics International* 43, no. 4 (2017): 3713-3719.
[3] Ohtake, Yasutoshi, Tamotsu Okamoto, Akira Yamada, Makoto Konagai, and Koki Saito. "Improved performance of Cu (InGa) Se_2 thin-film solar cells using evaporated Cd-free buffer layers." *Solar Energy Materials and Solar Cells* 49, no. 1-4 (1997): 269-275.
[4] Nakada, Tokio, and Masayuki Mizutani. "18% efficiency Cd-free Cu (In, Ga) Se_2 thin-film solar cells fabricated using chemical bath deposition (CBD)-ZnS buffer layers." *Japanese Journal of Applied Physics* 41, no. 2B (2002): L165.
[5] *Naghavi*, Negar, Stefani Spiering, Michael Powalla, Bruno Cavana, and Daniel Lincot. "High-efficiency copper indium gallium diselenide (CIGS) solar cells with indium sulfide buffer layers deposited by atomic layer chemical vapor deposition (ALCVD)." *Progress in Photovoltaics: Research and Applications* 11, no. 7 (2003): 437-443.
[6] Yousfi, E. B., T. Asikainen, V. Pietu, P. Cowache, M. Powalla, and D. Lincot. "Cadmium-free buffer layers deposited by atomic later epitaxy for copper indium diselenide solar cells." *Thin Solid Films* 361 (2000): 183-186.
[7] W. Eisele, A. Ennaoui, P. Schubert-Bischoff, M. Giersig, C. Pettenkofer, J. Krauser, M. Lux-Steiner, S. Zweigart, F. Karg, XPS, TEM and NRA investigations of Zn (Se,OH)/$Zn(OH)_2$ films on Cu(In,Ga)(S,Se) substrates for highly efficient solar cells, Sol. Energy Mater. Sol. Cell. 75 (2003) 17–26.
[8] Mikami, Rui, Hisashi Miyazaki, Tatunobu Abe, Akira Yamada, and Makoto Konagai. "Chemical bath deposited (CBD)-ZnO buffer layer for CIGS solar cells." In *Photovoltaic Energy Conversion, 2003. Proceedings of 3rd World Conference on*, vol. 1, pp. 519-522. IEEE, 2003.
[9] Kim, Ji Hye, Dong Hyeop Shin, Hyuk Sang Kwon, and Byung Tae Ahn. "Growth of Sn (O, S)$_2$ buffer layers and its application to Cu (In, Ga) Se_2 solar cells." *Current Applied Physics* 14, no. 12 (2014): 1803-1808.
[10] Amalraj, L., C. Sanjeeviraja, and M. Jayachandran. "Spray pyrolysised tin disulphide thin film and characterisation." *Journal of Crystal Growth* 234, no. 4 (2002): 683-689.
[11] Manohari, A. Gowri, K. Santhosh Kumar, Chaogang Lou, T. Mahalingam, and C. Manoharan. "Buffer layer of antimony doped tin disulphide thin films for heterojunction solar cells." *Materials Letters* 155 (2015): 121-124.
[12] Sharp, Laura, David Soltz, and B. A. Parkinson. "Growth and characterization of tin disulfide single crystals." *Crystal growth & design* 6, no. 6 (2006): 1523-1527.
[13] Price, Louise S., Ivan P. Parkin, Amanda ME Hardy, Robin JH Clark, Thomas G. Hibbert, and Kieran C. Molloy. "Atmospheric pressure chemical vapor deposition of tin sulfides (SnS, Sn_2S_3, and SnS_2) on glass." *Chemistry of materials* 11, no. 7 (1999): 1792-1799.
[14] Thangaraju, B., and P. Kaliannan. "Spray pyrolytic deposition and characterization of SnS and SnS_2 thin films." *Journal of Physics D: Applied Physics* 33, no. 9 (2000): 1054.

[15] Reddy, KT Ramakrishna, Gedi Sreedevi, Kottadi Ramya, and R. W. Miles. "Physical properties of nano-crystalline SnS_2 layers grown by chemical bath deposition." *Energy Procedia*15 (2012): 340-346.

[16] Cheng, L. L., M. H. Liu, S. C. Wang, M. X. Wang, G. D. Wang, Q. Y. Zhou, and Z. Q. Chen. "Nano-flower and nano-wall SnS_2 films fabricated with controllable shape and size by the PECVD method." *Semiconductor Science and Technology* 28, no. 1 (2012): 015020.

[17] Ray, Sekhar C., Malay K. Karanjai, and Dhruba DasGupta. "Structure and photoconductive properties of dip-deposited SnS and SnS_2 thin films and their conversion to tin dioxide by annealing in air." *Thin Solid Films* 350, no. 1-2 (1999): 72-78.

[18] Liu, Yongping, Peng Geng, Jixiang Wang, Zhishu Yang, Huidan Lu, Jiefeng Hai, Zhenhuan Lu, Dayong Fan, and Ming Li. "In-situ ion-exchange synthesis Ag2S modified SnS_2 nanosheets toward highly photocurrent response and photocatalytic activity." *Journal of colloid and interface science*512 (2018): 784-791.

[19] F. Li, L. Chen, G.P. Knowles, D.R. Macfarlane, J. Zhang, Hierarchical mesoporous SnO_2 nanosheets on carbon cloth: a robust and flexible electrocatalyst for CO_2 reduction with high efficiency and selectivity, Angew. Chem., Int. Ed. 56 (2017) 505–509.

[20] Fattah-Alhosseini, A., & Vafaeian, S. (2015). Comparison of electrochemical behavior between coarse-grained and fine-grained AISI 430 ferritic stainless steel by Mott–Schottky analysis and EIS measurements. Journal of Alloys and Compounds, 639, 301-307.

[21] Ullah, Shafi, Miguel Mollar, and Bernabé Marí. "Electrodeposition of $CuGaSe_2$ and $CuGaS_2$ thin films for photovoltaic applications." Journal of Solid-State Electrochemistry 20.8 (2016): 2251-2257.

[22] Ullah, Shafi, Hanif Ullah, Feriel Bouhjar, Miguel Mollar, Bernabé Marí, and Adil Chahboun. "Influence of Zinc Content in Ternary ZnCdS Films Deposited by Chemical Bath Deposition for Photovoltaic Applications." ECS Journal of Solid-State Science and Technology 7, no. 8 (2018): P345-P349.

[23] Wang, Xia, Xueying Li, Qiang Li, Hongsen Li, Jie Xu, Hong Wang, Guoxia Zhao et al. "Improved Electrochemical Performance Based on Nanostructured SnS_2@ CoS_2–rGO Composite Anode for Sodium-Ion Batteries." Nano-Micro Letters 10, no. 3 (2018): 46.

[24] Cifuentes, C., Botero, M., Romero, E., Calderon, C., & Gordillo, G. (2006). Optical and structural studies on SnS films grown by co-evaporation. Brazilian journal of physics, 36(3B), 1046-1049.

[25] Preethi, L. K., Mathews, T., Nand, M., Jha, S. N., Gopinath, C. S., & Dash, S. (2017). Band alignment and charge transfer pathway in three phase anatase-rutile-brookite TiO_2 nanotubes: An efficient photocatalyst for water splitting. Applied Catalysis B: Environmental, 218, 9-19.

[26] Xiang, Peng, Xiong Li, Heng Wang, Guanghui Liu, Ting Shu, Ziming Zhou, Zhiliang Ku et al. "Mesoporous nitrogen-doped TiO_2 sphere applied for quasi-solid-state dye-sensitized solar cell." Nanoscale research letters 6, no. 1 (2011): 606.